

See discussions, stats, and author profiles for this publication at: <https://www.researchgate.net/publication/262977620>

Real-Time Metabolic Analysis of Living Cancer Cells with Correlated Cellular Spectro-Microscopy.

ARTICLE *in* ANALYTICAL CHEMISTRY · JUNE 2014

Impact Factor: 5.64 · DOI: 10.1021/ac501561x · Source: PubMed

CITATIONS

3

READS

74

2 AUTHORS, INCLUDING:



[Luca Quaroni](#)

Institute of Nuclear Physics

84 PUBLICATIONS 1,017 CITATIONS

[SEE PROFILE](#)

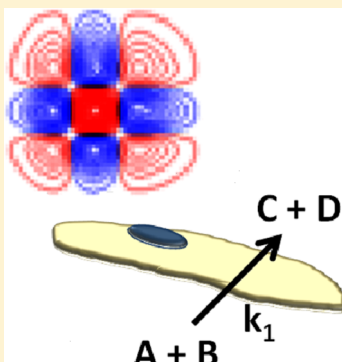
Real-Time Metabolic Analysis of Living Cancer Cells with Correlated Cellular Spectro-microscopy

Luca Quaroni*,† and Theodora Zlateva

Swiss Light Source, Paul Scherrer Institut, CH-5232 Villigen, Switzerland

 Supporting Information

ABSTRACT: In recent years, major efforts have been devoted to the application of microscopy with mid-infrared light to the study of living cells and tissue. Despite this interest, infrared (IR) microscopy has not realized its full potential in the molecular characterization of living systems. This is partly due to the fact that current approaches for data mining and analysis of IR absorption spectra have not evolved comparably to measurement technology and are not up to the interpretation of the complex spectra of living systems such as cells and tissue. In this work we show that the use of two-dimensional correlation spectroscopy coupled to IR absorption spectro-microscopy allows us to extract the spectral components of individual metabolites from time-resolved IR spectra of living cells. We call this method correlated cellular spectro-microscopy, and we implement it in the study of the glycolytic metabolism of cancer cells. We show that the method can detect intermediates of the glycolytic pathway, quantify their rate of formation, and correlate this with variations in pH, all in a single measurement. We propose the method as a useful tool for the quantitative description of metabolic processes in living cells and for the validation of drug candidates aimed at suppressing glycolysis in cancer cells.



Among techniques for the study of live biological systems, infrared (IR) absorption spectroscopy has received increasing attention in the past few years due to its general applicability, its viability as a fingerprinting technique for molecular identification, and its sensitivity to the structural parameters of a molecule.¹ In addition, its intrinsic non-destructiveness makes it an ideal tool for the real-time monitoring of biochemical processes in living organisms.² Most importantly, when implemented with microscopy optics, the technique allows probing of individual cells and subcellular compartments, thus providing both spatial and temporal representations of biochemistry *in vivo*.^{2,3} To date, the potential of IR microscopy in the study of living cells and tissue has not been fully realized. Despite its rich and detailed content in terms of compositional and structural information, the technique, in its current application to living systems, is mostly used to characterize the content of classes of macromolecules, such as proteins, lipids, and nucleic acids. Reliable assignment of the spectra of individual molecular components is still a challenge and is successful only in specific cases, in the presence of high concentrations of individual molecules. In this work we describe an approach to analyze the spectra of living cells that overcomes these limitations and allows systematic extraction of the compositional changes associated with metabolic processes and identification of individual metabolites. We call the method correlated cellular spectro-microscopy (CSM) because of its reliance on the correlation properties of spectral changes in an evolving system.

The specific case addressed in this paper is the glycolytic metabolism of cancer cells. The choice of system highlights the usefulness of the method in the study of cancer metabolism and

the tumor environment. In recent years, the subject has received renewed attention as the basis of a strategy to control or suppress tumor cells by targeting elements of their specific metabolic pathways.^{4,5} CSM can provide a wealth of information necessary to characterize the metabolism of cancer, including identification of metabolites, quantification of rates of production, and real-time measurement of pH variations. In this context, we put forward CSM as a valuable platform for the quantitative testing of new drugs and therapies.

EXPERIMENTAL SECTION

Chemicals. All chemicals, except for cellular growth media, were purchased from Sigma-Aldrich and were of the purest available grade. Cell culture supplies were purchased from Invitrogen.

Cell Culture. A549 cells (Human Caucasian Lung Carcinoma; ECACC catalog no. 86012804) were cultured directly on CaF₂ windows. Details of the culture protocol are provided as Supporting Information. For Fourier transform infrared (FTIR) spectro-microscopy measurements, the cell-coated window was transferred to a custom-built solution sample holder kept at 37 °C.

Sample Holder for FTIR Measurements on Cells. The sample holder is a variation of a sandwich design, with two optical windows separated by a spacer.² Prior to the experiment, the cell-coated window was placed into the holder

Received: February 10, 2014

Accepted: June 10, 2014

Published: June 10, 2014



with the growth medium. The spacer was superimposed, and the second window was placed on top of the stack, followed by gentle tightening. No perfusion of the sample was performed. The viability of cells in the holder has been tested by using Trypan Blue.⁶ Additional details are provided as Supporting Information.

FTIR Spectro-microscopy Experiments. FTIR spectro-microscopy measurements were performed using the microscope setup of beamline X01DC of the Swiss Light Source with the internal source. The setup comprises a Bruker Vertex 70v interferometer (Bruker Optics) and a Bruker Hyperion 3000 microscope.

The IR beam was then moved to the location of a cell cluster for the sample single-channel measurements described below. The confocal aperture was set to $100 \times 100 \mu\text{m}^2$ and positioned to enclose a cluster of 6–8 adherent cells. Spectra are plotted as differences from the first spectrum.

Additional details on experimental procedures are provided as Supporting Information.

Data Analysis. Data workup was performed using the software package OPUS 7.0 (Bruker Optics). Second derivatives were calculated using nine-point Savitzky–Golay smoothing. Two-dimensional correlation spectroscopy (2D-COS) analysis was performed using the program MIDAS, written by Elise Normand, University of Saskatchewan. Contour levels in the 2D-COS plots are 1/128 of the total not-normalized scale amplitude, except for Supporting Information Figure SI4, for which they are 1/64.

RESULTS

Figure 1 shows a schematic representation of the individual steps involved in CSM. The overall strategy involves measuring over time IR absorption spectra, which contain all the information about the biochemistry of the sample. The spectra are processed using 2D-COS analysis to spread the spectral variations over two dimensions and to identify individual molecules. On the basis of these assignments, kinetic information can be extracted about the formation and consumption of individual molecules.

We implement CSM by measuring metabolic activity in cells of the A549 human lung adenocarcinoma cell line. Figure 2A shows the difference spectra from a cluster of A549 cells recorded during the first 90 min after insertion into the sample holder, while Figure 2B shows the corresponding second-derivative spectra. The spectra of Figure 2A show marked variations in baseline that can be stronger in amplitude than other spectral changes. These variations are common in measurements of living cells and are due to changes in the optical properties of the sample that occur over time, because of the movement of cells within the aperture, changes in cell shape, or changes in the chemical composition of the cell or medium (variations in pH, variations in the concentration of the most abundant biomolecules, formation of extracellular concentration gradients), all of which affect its refractive index. These changes cause a variation of throughput to the detector and cause apparent changes in absorbance in the spectra.^{8,7} We reduce the relative contribution of baseline variations by working with the second derivative of the absorbance spectra.⁹ As a result, the strong baseline variations observed in the spectra of Figure 2A are absent or negligible in the second-derivative traces of Figure 2B, providing a spectral evolution profile which is dominated by contributions from light absorption. The trade-off for this baseline correction method

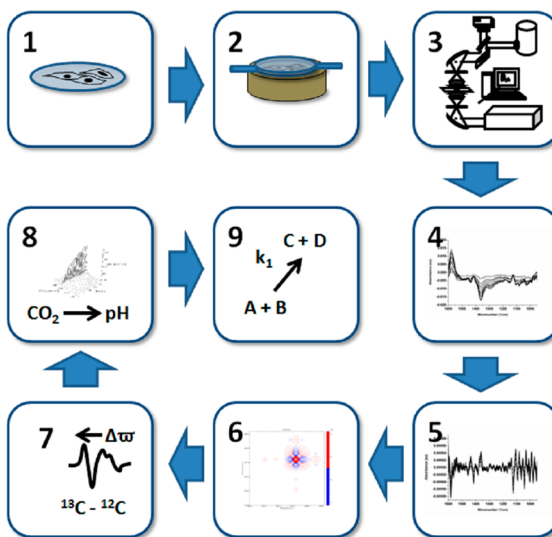


Figure 1. Schematic representation of the experimental and data-processing steps for correlated cellular spectro-microscopy of live cells: 1, cells are cultured directly on optical windows that are transparent to light in the mid-IR spectral region and nontoxic to the cells; 2, when the desired growth stage is reached, the cells are transferred to a temperature-controlled sample holder for IR microscopy; 3, the sample holder is moved to an IR microscope, the region of interest is imaged using the microscope objectives and selected using the confocal apertures of the microscope, and IR absorption measurements are performed sequentially on this region for the duration of the process which is under study; 4, spectral information is plotted as difference absorption spectra vs time after subtraction of the first spectrum from the following ones; 5, difference spectra are converted to their second-derivative form to reduce the contribution from baseline variations; 6, second-derivative plots are analyzed using correlation analysis, and the correlation plots are used to identify bands arising from the individual chromophores, to assign sequences of reaction events, and to provide a spectral and temporal fingerprint of the chemistry at play; 7, isotopic labeling of nutrients or drugs can be used in pair with 2D-COS plots both to help with band assignment and to obtain information about reaction mechanisms and metabolic pathways; 8, once assignments and chromophore identification have been completed in the space of 2D-COS diagrams, the time-resolved plots of second derivatives can be used to extract rates of formation and decomposition of specific chromophores; and 9, the end result is a conversion of the complex spectral variations of the cellular system into a quantitative description of reactant and product evolution.

is increased spectral complexity, due to the overlapping contribution of the side bands from the second derivative of Gaussian and Lorentzian bands.

We use the correlation properties of the spectral components to overcome the complexity of cellular second-derivative spectra and to extract a representation of the molecular processes in the cell. Analysis of the individual, one-dimensional spectra of Figure 2B and assignment of all but the strongest spectral contributions are daunting. However, when analyzing time sequences of spectra, we can take advantage of constraints imposed on spectral complexity by existing correlations between molecular species and their spectral features. For this purpose we use 2D-COS analysis.

Correlation Analysis of Cellular Reactions. 2D-COS was introduced by Isao Noda as a method of data analysis to quantify and parametrize the relationship between spectral properties that vary as a function of an evolving parameter or physical quantity, such as time.¹⁰ The application of 2D-COS to

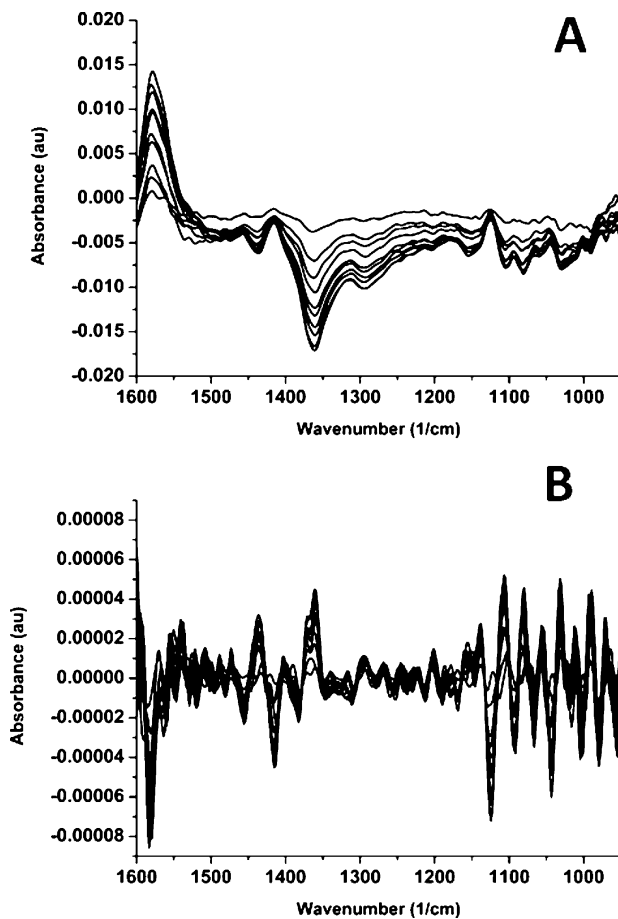


Figure 2. (A) Difference spectra from a cluster of live A549 cells recorded during the first 90 min. (B) Second derivative of the absorption spectra from panel A. For clarity, only spectra recorded every 10 min are shown. Spectra are plotted as differences from the first spectrum. Positive bands in panel A correspond to species that accumulate, and negative bands correspond to species that are consumed. Signs are inverted in second-derivative plots. Therefore, in panel B, positive bands correspond to species that accumulate, and negative bands correspond to species that are consumed.

a data set involves calculation of the correlation function of the evolving spectral profiles followed by application to the latter of a 2D Fourier transform algorithm. The result is a complex function of two wavenumber variables that is plotted as separate real and imaginary components. The real component is called the synchronous plot, and the imaginary component is called the asynchronous plot. Figure SI1 in the Supporting Information shows the synchronous and asynchronous plots from the set of spectral second derivatives of Figure 2B.

The synchronous plot represents correlations between pairs of wavenumbers that are changing fully in phase or with opposite phase. Two peaks that change in phase in the spectra of Figure 2B give rise to positive “correlation peaks” in the synchronous plot, on both sides of the diagonal. Peaks that change with opposite phase give negative correlation peaks.

The asynchronous plot represents correlations between pairs of wavenumbers that have an out-of-phase relationship. Two peaks that change out-of-phase in the spectra of Figure 2B give rise to a positive correlation peak on one side of the diagonal and a negative peak on the opposite side. The sign of the correlation peaks is a function of the sequence of the changes.

Quaroni et al.⁷ have shown that the correlation properties of spectral changes arising from the same chromophore allow us to assign the full set of bands belonging to that chromophore. In this context we use the word *chromophore* to indicate a set of bands that change in perfect synchrony, thus displaying positive correlation peaks in the synchronous plot and no correlation peaks in the asynchronous plot. The bands of one chromophore could be due to one specific molecule or to several molecules that have the same time evolution within the time resolution afforded by the measurement.

By applying these constraints, the hundreds of peaks in the plots of Figure 3 can be reduced to a relatively small set of

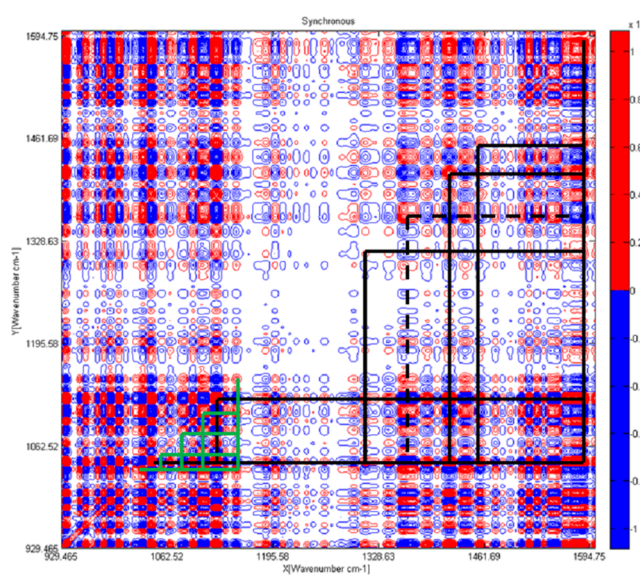


Figure 3. Identification of glucose and lactate: 2D-COS synchronous plot of the spectral set in Figure 2B. Peaks assigned to lactate are highlighted in black, and peaks assigned to glucose are highlighted in green. The dotted line indicates a lactate band that has the wrong correlation because of overlap with a strong bicarbonate band.

chromophores. Fingerprinting analysis of the peaks of individual chromophores can then lead to easy identification of specific molecules. Analysis of the correlation properties of bands also allows identifying the spectral contribution of the side bands in the second derivative of Lorentzian/Gaussian peaks, thus greatly simplifying assignments.

Figure 3 shows an example of identification following these precepts. Herein we mark the peaks that satisfy the conditions for synchrony laid out above for two of the molecular components of the system. Taking advantage of the peaks assigned to them, we can easily apply fingerprinting analysis to identify these two components as lactate and glucose. The phase relationship between the two is revealed by the negative sign of their correlation peaks in the synchronous plot and shows that the consumption of glucose corresponds to the formation of lactate. The presence of correlation peaks in the asynchronous plot and their sign reveal the existence of a delay between the consumption of glucose and the formation of lactate. This is expected, since glucose is the first substrate of glycolysis and lactate is the final product of fermentation. Similar relationships can be built for all other molecule pairs in the evolving system.

Detection of Metabolic Intermediates. Iteration of this analysis allows identification of several molecules from the plots

Table 1. Molecules Detected in A549 Cells^a

Peak Position (cm ⁻¹)	Lactate (Y)	Pyruvate (Y)	3-PG (Y)	2-PG (Y)	PEP (N†)	G3P (Y)	ATP (N†)	Glucose (Y)	DPPC (N)	RNA (Y)	PO4 (N†)	Amides (Y)
937												
											† 942	
955		954		950			950					
962						963						
								(-) 970				
976			977 vs									
984		982		980								
995							999	994				
1003				1003								
1014			1016	1015		1009						
1024		1022					1022					
1036								1034				
1044	1041		1044	1047		1043						
1059								1058				
1069												
						† 1075 vs				† 1077 vs		
1084			1084 s	1083 s		1084 s		1080		1086		
					†1091 vs				† 1091 vs			
1100							1097					
1107						1109		1108				
1111			1111									
1127	1128			1126		1129	1125					
1138												
1152								1150				† 1159
1167												
1177		1177				1180						
1189				1184								
1202					1198							
1212												
1223												
1241							1244		1242	1244		
1262												
1285												
1299												
1314	1314			1314								
1328			1331									
1363	*1366	1358	1364	1362								
1376									1378			
1394		1394										
1405												
1425	1420	1425	1420	1421			1425					
1440												
1459	1457		1458	1458								
								(-) 1467				
1479												
1512							1510					
1521												
1531												
1537												

Table 1. continued

Peak Position (cm ⁻¹)	Lactate (Y)	Pyruvate (Y)	3-PG (Y)	2-PG (Y)	PEP (N†)	G3P (Y)	ATP (N†)	Glucose (Y)	DPPC (N)	RNA (Y)	PO ₄ (N†)	Amides (Y)
1548												
1566												
1579	1579											
to			1587									
1597												

^aMetabolites and other molecular species identified from the 2D-COS plots of Figure 3. Abbreviations: 2-PG, 2-phosphoglycerate; 3-PG, 3-phosphoglycerate; PEP, phosphoenolpyruvate; G3P, glyceraldehyde-3-phosphate; PO₄, mono and dibasic phosphate; DPPC, dipalmytoilphosphatidylcholine (as a prototype phospholipid); RNA, Ribonucleic Acid. The letter (Y) together with the name of a molecule indicates that the molecule is detected in the 2D-COS plots. The letter (N) indicates that it is not. The indication VS (very strong) or S (strong) together with a wavenumber entry is used to indicate the intensity of bands in the spectra of the pure compounds in solution. † indicates bands that are observed only in variance scaled synchronous plots. * indicates a lactate band which is covered by a stronger band from bicarbonate. Black cells indicate extended spectral regions where Amide bands are known to absorb.

of Figure SI1. The results are summarized in Table 1. The wavenumber listing in the left column indicates peaks that are observed in the 2D-COS plots. The list is based on the peaks identified in the synchronous and asynchronous plots. In addition, complex multiplets, which may appear as a single band in the synchronous plot, are split into their components on the basis of analysis of the asynchronous plot. The column headings list the metabolites and other significant biomolecules that may be present at detectable concentrations and contribute to the IR spectrum. Several glycolytic metabolites are successfully observed.¹¹

Entries preceded by a minus sign in parentheses indicate bands of a compound that are observed in solution spectra of the pure compound but not present in 2D-COS plots. Entries marked with an asterisk indicate bands that have an unexpected phase relationship in the synchronous plot, because of overlap with strong bands from other molecules, but whose assignment is nonetheless supported by the observation of the asynchronous plot. As an example, there appears to be one peak at 1363 cm⁻¹ in the synchronous plot, but this is revealed to be a multiplet in the asynchronous plot: the 1365 cm⁻¹ band of lactate is one component of this multiplet, which is nonetheless dominated by the strong contribution of bicarbonate. Because of the latter, the overall absorbance change at this frequency is not in phase with that of other lactate bands.

Several small molecules contribute to the spectra that belong to the glycolytic pathway, such as pyruvate, 2-phosphoglycerate, and 3-phosphoglycerate. The dominant contributions are due to lactate, the end product of fermentation, and glucose, the substrate for glycolysis in the growth medium. The detection of the less concentrated metabolites is remarkable, since their expected concentrations are close to the detection limit of the technique. It is also notable that ATP is not observed in these plots, since its strongest peak at 1075 cm⁻¹ is missing. Bands from free phosphate ions are also missing, indicating that their concentrations are not changing in a detectable way over time. Nonetheless, as noted later, these bands can be detected as weak components in variance-scaled correlation plots.

Changes in biomolecules other than metabolites can also be monitored using the same measurements. It is notable that no changes are seen in phospholipid bands throughout the measurement. In contrast, we can see changes in bands assigned to RNA, as indicated by the peak at 1244 cm⁻¹. Cellular proteins and polypeptides also give rise to strong absorption bands in this spectral region.¹² The strongest

contribution, from the Amide I band, is covered by water absorption and is not included in this analysis. In 15 μm thick samples, absorption by the bending mode of water considerably increases noise levels around 1640 cm⁻¹, preventing the use of the second-derivative spectra around this region. Other regions where amide bands appear are collectively represented with black cells in Table 1. Several peaks from the 2D-COS plots that have not been assigned to any metabolites or other small molecules are present in these regions. Changes in peptide bands indicate that variations in the composition of the cellular proteome take place in parallel with metabolic turnover. The fact that changes in protein bands occur in parallel with those of RNA bands also suggests that protein synthesis is taking place.

Variance-Scaled Correlation Analysis. The correlation plots in Figure SI1 are calculated using the uncorrected variation of absorbance at each wavenumber. This approach provides correlation plots that are dominated by bands that display larger absorption changes during the selected measurement interval. Normalizing the absorbance scale relative to the variance of each band allows overcoming this limitation. The resulting variance-scaled plots are dominated by correlation between bands, irrespective of band intensity and concentration changes. Figure SI2 shows the variance-scaled synchronous plot for the spectra in Figure 2. Several new bands appear, arising from weaker spectral variations that were undetected in the unscaled plots. These include bands at 1075, 1091, and 1159 cm⁻¹ that can be assigned to absorption bands from ATP and phosphate ions, which were undetected in the analysis of uncorrected plots. This observation suggests that these molecules do display concentration changes, however small, during the course of the measurement.

Despite the apparent usefulness of variance-scaled plots in extracting information about minor spectral components, their complexity when used for the analysis of a cellular system imposes severe limitations. In the specific case of the variance scaled asynchronous plot, this complexity implies that in most cases it is not possible to clearly observe the positions with zero correlation intensity, as required for the safe assignment of bands to one chromophore. Therefore, the assignment of bands to ATP and phosphate, as discussed above, must rely on *a priori* knowledge of the system.

Isotopic Substitution. The use of isotopically substituted molecules is a traditional tool in both vibrational spectroscopy and physiology, for band assignment, molecular identification, and molecular tracking. We show that CSM allows easy

application of isotopic substitution techniques in cellular spectra. Supporting Information Figure SI4A displays the spectral changes of a cluster of A549 cells where glucose labeled with ^{13}C in the 6C position has been incorporated into the growth medium during the exponential phase. Panel B shows the corresponding second-derivative traces. Panels C and D show the resulting synchronous and asynchronous 2D-COS plots.

The spectra obtained with ^{13}C glucose are qualitatively similar to the ones obtained from cells cultured in the presence of glucose with normal isotopic abundance. The main differences between the spectra of glucose with normal isotopic substitution and glucose with ^{13}C in position six (6- ^{13}C glucose) are expected from three bands. The band at 1150 cm^{-1} shifts to 1128 cm^{-1} and the band at 1034 cm^{-1} shifts to 1025 cm^{-1} with the introduction of ^{13}C . In addition, a band at 1075 cm^{-1} increases in intensity with the introduction of ^{13}C (see Supporting Information Figure SI3). These isotopic shifts are difficult to identify unequivocally in the spectra of Figure SI4A because of a combination of baseline effects and weak absorption differences. In contrast, identification of the full band pattern of ^{13}C glucose is possible in the 2D-COS plot of Figure SI4C.

Variations of CO_2 , HCO_3^- , and pH. Metabolic acidification of the cytoplasm and medium leads to the protonation of aqueous bicarbonate ions and the formation of aqueous carbon dioxide ($\text{CO}_{2(\text{aq})}$). This appears as a strong, sharp peak at 2343 cm^{-1} that evolves over time, as shown in Figure 4.¹³

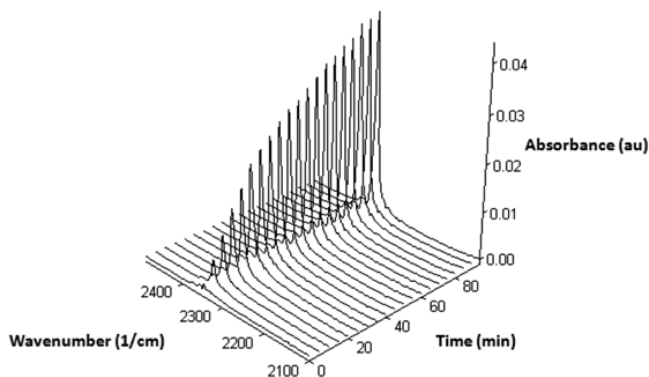


Figure 4. Formation of aqueous CO_2 in cells and medium: increase of the absorption band at 2343 cm^{-1} from $\text{CO}_{2(\text{aq})}$ associated with the acidification of the cells and the surrounding medium. Spectra are plotted every 10 min for clarity. This corresponds to a drop in pH of -1.6 pH units over a 60 min period.

The intensity of the peak of $\text{CO}_{2(\text{aq})}$ can be used to indirectly monitor the acidification of the sample, as previously reported.¹⁴ Similar information can be obtained from the decrease in concentration of aqueous bicarbonate ($\text{HCO}_3^-_{(\text{aq})}$), given by its absorption change at 1362 cm^{-1} .¹³ For this specific experiment, the variation is calculated to be -1.6 pH units over a 60 min period. The sharp drop in pH is expected when considering that the cells and surrounding medium are enclosed in a volume which is $15\text{ }\mu\text{m}$ thick and easily acidified by the release of metabolic H^+ ions.

Kinetic Measurements. Band assignment can be followed by quantitative assessment of their time evolution, using standard procedures of curve fitting. As an example, fitting of an exponential curve to the second-derivative peak at 1126 cm^{-1} , corresponding to lactate formation, provides a rate constant for

lactate formation of 86 min^{-1} . The fit is shown in Supporting Information Figure SI5. Using a coefficient of $\epsilon_{2\text{ndDer}} = 4.4 \times 10^{-4}\text{ M}^{-1}\text{ }\mu\text{m}^{-1}$ for the second-derivative absorption of lactate (see Supporting Information), we obtain a value of 17 mM min^{-1} for the initial rate of formation of lactate in the probed volume. A similar treatment can be applied to the bands from other molecules to obtain a full kinetic description of the system.

■ DISCUSSION

The compositional complexity of biological systems is a challenge to the introduction of new analytical methods, which need to mature to a stage where they can extract and handle hundreds of variables with a single experiment. IR absorption spectroscopy is currently still facing this challenge. Part of the difficulty is that current approaches to data mining and analysis of IR absorption spectra have not evolved comparably to measurement technology and struggle with the interpretation of the complex spectra of living cells and tissue. Molecular analysis of cells and tissue via IR absorption spectra is typically based on functional group analysis of one-dimensional spectra. The complexity of a cellular IR absorption spectrum makes this approach inadequate because of the unresolved overlap of multiple bands in a narrow spectral range. In addition, it often results in wrong, contradictory, or untestable assignments, because of its reliance on a small number of peaks, or even on single peaks, which are amenable to multiple assignments. Successful interpretation of IR spectra often requires the use of additional analytical techniques or the use of established knowledge about the sample. In addition, most spectral features, particularly weaker ones, are left unassigned, thus resulting in the waste of most of the information content from an experiment.

The introduction of automated methods of multivariate data analysis has provided an improvement in the capability to classify and analyze spectral data in an automated, objective, and reliable way. Nonetheless, the identity of individual molecular species is lost when applying multivariate methods, with consequent loss of information concerning composition and molecular structure. As a consequence, multivariate analysis has been successfully used for histopathologic recognition in diagnostic applications of IR spectroscopy^{15,16} but has had little impact on experiments where detailed molecular characterization of the sample is the objective.

IR absorption spectroscopy of pure phases or of simple mixtures has been used for decades for molecular identification via fingerprinting analysis of molecules. The practice relies on the uniqueness of the IR absorption spectra of molecular species. To be reliable, fingerprinting needs to be done using the complete pattern of bands of a molecule or, at the very least, a substantial fraction of them. CSM allows the identification of the full set of bands associated with a molecular chromophore. Therefore, it allows reliably extending the practice of fingerprinting to the identification of molecules in cellular samples, including species that are not dominant components of the system. The viability of the approach is demonstrated by the identification of the intermediates of glycolysis during the exponential growth phase, as summarized in Table 1. The less abundant metabolites, such as pyruvate, would not be identifiable in one-dimensional spectra because of the weakness of the signal and the lack of specific functional groups to facilitate their identification.

In this context, CSM constitutes a major improvement in the capability of IR absorption spectroscopy to extract the complex molecular pattern of reactions in live cells. The improved reliability of assignments creates an opportunity to make IR absorption microscopy a real discovery technique, since it allows recovery of the full spectrum of unknown or unexpected molecules, thus providing an opportunity for their identification without the use of additional techniques and of pre-existing knowledge of the system. This is impossible or difficult when identifying molecules on the basis of single bands. For example, a band at $1124\text{--}1128\text{ cm}^{-1}$ is observed with varying intensity in many samples of cells and tissue. Some examples are found in the literature.^{17–19} This band can arise from several different metabolites, as shown in Table 1. Its reliable assignment to lactate in our experiments is possible by observing the full set of lactate bands in the mid-IR region. The same analysis also shows that this band overlaps with the contributions from phosphoglycerate, glyceraldehydes-3-phosphate, and ATP, all of which should be taken into account if quantitative information needs to be extracted from it.

An additional example of how CSM can help to clarify cellular spectral complexity is given by the multiplets around 1085 and 1245 cm^{-1} . When analyzed individually, according to the practice of functional group analysis, these bands are often assigned to vibrations of the phosphate ester group in nucleic acids.^{20,21} In some cases, either or both of these bands are assigned to phospholipid headgroups,⁷ to phosphoproteins,^{22,23} or to all of them.²⁴ Other assignments are often neglected. Our analysis shows that the situation is very complex. Several phosphate-containing species and molecules containing C–O bonds, all present at detectable concentrations in the cell, contribute to absorbance in this region.^{25,18,26} Analysis of single bands is not capable of separating their individual contributions, and extreme care should be applied whenever assigning these bands.

It is to be noted that principal component analysis (PCA)²⁷ could also be applied to the identification of bands arising from the same chromophore, which would appear as a single principal component. However, the output of PCA analysis does not retain any information about the sequence of events in the sample. In contrast, an important feature of CSM is that the asynchronous plots contain information about the time sequence of events that relate molecular species in the sample. The sequence of formation or consumption of two species affects the sign of the off-diagonal peaks that relate their spectra in the asynchronous plots.¹⁰ Therefore, the combined synchronous and asynchronous plots contain precious information on the sequence of reactions. This is expressed in “sequential order rules” and is a potentially rich source of information about cellular pathways. Nonetheless, care should be taken when extracting sequential information. It has been shown that the interpretation is not univocal and depends on the relative kinetics of the changes.²⁸ Therefore, previous information about the time evolution of the processes under study must be available for a correct interpretation of event sequences. In this experiment, the second-derivative kinetic traces are sufficiently clear to provide that information.

It is important to stress that CSM probes the variation in concentration of molecular species, not their absolute concentration. Molecules that maintain a constant concentration under steady-state or homeostatic conditions are not detected. Molecules other than the initial substrates and the final products of the metabolic processes, glucose and lactate in

our experiments, can be detected only because steady-state conditions are avoided. The presence of a time lag between glucose consumption and lactate formation, as indicated by correlation analysis, has the same origin. This is achieved by measuring changes only over the first hour after introducing the sample into the chamber, before cells have adjusted to their new environment and while anoxic conditions are developing. Failure to satisfy this condition is also the reason for the difficulty in detecting some metabolites, such as ATP and phosphate ions, for which nearly homeostatic conditions are ensured by their shared participation in multiple metabolic networks. 2D-COS plots calculated from spectra recorded at later times (data not shown), when the cell culture has stabilized and steady-state conditions are achieved from most intermediates, are completely dominated by peaks from lactate and glucose.

Cancer cells are known to use glycolysis as the main pathway for energy production, even under aerobic conditions.²⁹ The experimental conditions used for our measurements, characterized by increasing anoxia and the use of glucose as the main nutrient in the sample, have been chosen to further enhance the use of the glycolytic pathway.³⁰ Glycolytic intermediates are expected to be more abundant and to dominate spectral plots and 2D-COS plots. The results of our analysis show that this is indeed the case and allow us to assign the majority of the bands observed in the 2D-COS plots to such intermediates. The observed acidification is also a known consequence of glycolytic turnover.³⁰ Nonetheless, several bands, mostly weaker ones, are as yet unassigned. These bands can arise from a variety of cellular processes, including the activity of metabolic networks other than glycolysis, and their assignment will be the subject of future research.

We show that CSM is compatible with the use of isotopic substitution for band assignment and the identification of molecular components. The use of isotopic shifts to confirm band assignments is a standard procedure in vibrational spectroscopy. Nonetheless, its use has been limited or neglected in IR absorption experiments on living cells. Part of the reason is the difficulty in identifying an isotopically shifted band in the complex absorption pattern from a cell, particularly when it arises from a minor component. CSM greatly facilitates the observation of isotopic shifts in two ways. First, the spreading out of bands over two dimensions allows resolving weaker components. Second, the collective identification of all detectable bands from the same molecule facilitates the identification of an isotopically shifted band.

In this work, isotopic labeling has been used as a proof concept, to demonstrate its use in molecular identification and band assignment. However, an important future extension of the method is the study of isotopic flow through metabolic networks. Isotopic tracers are a common tool in metabolic studies, where they provide rich information on the identity of substrate pools, on the mechanism of individual reactions, and on the sequential relationship between reactions. It is notable that, under the experimental conditions used in the present work, labeled glycolytic intermediates are not observed. Extended incubation of cells with $6\text{-}^{13}\text{C}$ -glucose gives rise to an array of labeled intermediates, most of which have an isotopic enrichment of the order of 10% or less, which are difficult to detect in 2D-COS plots.³¹ Incubation of cells with fully labeled glucose ($^{13}\text{C}_6$ -glucose) will be required to detect distribution of the isotopic label among intermediates.

The parallel measurement of variations in the concentration of $\text{CO}_{2(\text{aq})}/\text{HCO}_3^{-\text{(aq)}}$ and the secondary measurement of pH from spectroscopic data are also very valuable features of CSM. Acidification of the extracellular environment is associated with glycolysis and is the cause of the acidic environment that surrounds most cancer cells. These quantities are important elements in the characterization of metabolic activity and are related to some of the proposed pharmacological targets for metabolic-based cancer therapies.⁵ The concept of measuring physiological pH from the concentration of $\text{CO}_{2(\text{aq})}/\text{HCO}_3^{-\text{(aq)}}$ *in vivo* has already been implemented in hyperpolarized ^{13}C NMR experiments,³² which have been very successful in the study of the tumor microenvironment.³³ The implementation via IR microscopy has similar advantages but also provides additional features, such as cellular resolution and the parallel measurement of pH values together with all the other spectroscopic properties of the sample. This feature allows quantitative correlation of metabolic activity and cellular pH in selected locations within the sample.

Figure S11 shows the results obtained by measuring one single-cell cluster in a specific sample. To assess the degree of reproducibility, the measurements were repeated several times using the same or similar experimental conditions. The results of a set of such measurements from the same batch of cell cultures are reported and discussed in the Supporting Information (Figure SI6). It is important to highlight that some of the molecules detected in these experiments are present both in the extracellular medium and in the cytoplasm, such as lactate and glucose. In contrast, several intermediates are confined to the cytoplasm, including phosphate esters and anhydrides. As a consequence, the relative contribution of the various molecules to the average spectrum of the cell cluster is greatly affected by the footprint of the cluster within the measurement aperture. The use of an imaging configuration is necessary to quantitatively separate the contribution of species in the extracellular medium and the cytoplasm. An approach that couples IR imaging and 2D-COS has already been introduced.³⁴ Its implementation to an evolving cellular system, after adapting to a process that lacks periodicity, will be the subject of future experiments.

CONCLUSIONS

We introduce correlated cellular spectro-microscopy (CSM) to detect metabolites and other biomolecules that participate in the biochemistry of living cells. This is the first approach that allows the simplification and systematic analysis of complex cellular infrared reaction spectra. It reduces the spectroscopic changes in a living cellular system to a series of reactions involving specific molecules. In so doing, it affords the possibility of identifying specific reacting molecules within cells by spectral fingerprinting. It is not limited by the complexity of the reaction system, allowing in principle to identify as many molecular species as there are reacting components. Its intrinsic limitation is the sensitivity of IR absorption measurements, which restricts it to variations of concentration in the millimolar range. We show that the method is suitable for real-time metabolome analysis that includes rates of metabolite formation and consumption. The resulting representation displays the compositional, structural, and dynamic information associated with cellular biochemistry in a form which is easy to interpret and easy to mine, with the main limitation being the detection limit of IR absorption spectroscopy for specific bands. We test CSM in the

identification of intermediates in the glycolytic and fermentative metabolism of cancer cells. However, the applicability of the method is general, and the same experimental configuration can be used to address other processes. Promising fields of application include cellular physiology, network biology, pharmacodynamics, diagnostics, and cellular biophysics.

ASSOCIATED CONTENT

S Supporting Information

Additional information as noted in text. This material is available free of charge via the Internet at <http://pubs.acs.org>.

AUTHOR INFORMATION

Corresponding Author

*E-mail: quaroni@bluewin.ch

Present Address

[†]Functional Genomics Center Zürich, 190 Winterthurerstrasse, CH 8057 Zürich Switzerland

Notes

The authors declare no competing financial interest.

ACKNOWLEDGMENTS

We are grateful to Blagoj Sarafimov, Swiss Light Source, for design and construction of the sample holder. We are grateful to Elise Normand, University of Saskatchewan, for support with the program MIDAS. This work was financed by internal funding of the Swiss Light Source.

REFERENCES

- (1) Moss, D., Ed. *Biomedical Applications of Synchrotron Infrared Microspectroscopy*; Royal Society of Chemistry: Cambridge, 2011.
- (2) Quaroni, L.; Zlateva, T. *Analyst* **2011**, *136*, 3219–3232.
- (3) Holman, H.-Y. N.; Bechtel, H. A.; Hao, Z.; Martin, M. C. *Anal. Chem.* **2011**, *82*, 8757–8765.
- (4) Kim, J. W.; Dang, C. V. *Cancer Res.* **2006**, *66*, 8927–8930.
- (5) Parks, S. K.; Chiche, J.; Pouyssegur, J. *Nature Reviews Cancer* **2013**, *13*, 611–623.
- (6) Kreuzer, H. W.; Quaroni, L.; Podlesak, D. W.; Zlateva, T.; Bollinger, N.; McAllister, A.; Lott, M. J.; Hegg, E. L. *PLoS One* **2012**, *7*, e39685.
- (7) Quaroni, L.; Zlateva, T.; Normand, E. *Anal. Chem.* **2011**, *83*, 7371–7380.
- (8) Davis, B. J.; Carney, P. S.; Bhargava, R. *Anal. Chem.* **2010**, *82*, 3487–3499.
- (9) Romeo, M.; Diem, M. *Vib. Spectrosc.* **2005**, *38*, 129–132.
- (10) Noda, I. *Front. Mol. Spectrosc.* **2009**, *367*–381.
- (11) Bar-Even, A.; Flamholz, A.; Noor, E.; Milo, R. *Nat. Chem. Biol.* **2012**, *8*, 509–517.
- (12) Barth, A. *Biochim. Biophys. Acta—Bioenergetics* **2007**, *1767*, 1073–1101.
- (13) Falk, M.; Miller, A. G. *Vib. Spectrosc.* **1992**, *4*, 105–108.
- (14) Carbone, M.; Zlateva, T.; Quaroni, L. *Biochim. Biophys. Acta—Gen. Subjects* **2013**, *1830*, 2989–2993.
- (15) Fernandez, D. C.; Bhargava, R.; Hewitt, S. M.; Levin, I. W. *Nat. Biotechnol.* **2005**, *23*, 469–474.
- (16) Krafft, C.; Steiner, G.; Beleites, C.; Salzer, R. *J. Biophotonics* **2009**, *2*, 13–28.
- (17) Diem, M.; Romeo, M. J.; Boydston-White, S.; Matthaus, C. In *Spectrochemical Analysis Using Infrared Multichannel Detectors*; Bhargava, R., Levin, I. W., Eds.; Wiley-Blackwell: Hoboken, NJ, 2005: Chap. 9, pp 189–203.
- (18) Quaroni, L.; Casson, A. G. *Analyst (Cambridge, U.K.)* **2009**, *134*, 1240–1246.
- (19) Quaroni, L.; Christensen, C. R.; Chen, B.; Vogl, W.; Monsalve, M. V. *Microsc. Microanal.* **2013**, *19*, 565–575.

- (20) Walsh, M. J.; Fellous, T. G.; Hammiche, A.; Lin, W. R.; Fullwood, N. J.; Grude, O.; Bahrami, F.; Nicholson, J. M.; Cotte, M.; Susini, J.; Pollock, H. M.; Brittan, M.; Martin-Hirsch, P. L.; Alison, M. R.; Martin, F. L. *Stem Cells* **2008**, *26*, 108–118.
- (21) Whelan, D. R.; Bambery, K. R.; Puskar, L.; McNaughton, D.; Wood, B. R. *J. Biophotonics* **2012**, *6*, 775–784.
- (22) Vileno, B.; Jeney, S.; Sienkiewicz, A.; Marcoux, P. R.; Miller, L. M.; Forro, L. *Biophys. Chem.* **2010**, *152*, 164–169.
- (23) Chen, L.; Holman, H.-Y. N.; Hao, Z.; Bechtel, H. A.; Martin, M. C.; Wu, C.; Chu, S. *Anal. Chem.* **2012**, *84*, 4118–4125.
- (24) Mourant, J. R.; Gibson, R. R.; Johnson, T. M.; Carpenter, S.; Short, K. W.; Yamada, Y. R.; Freyer, J. P. *Phys. Med. Biol.* **2003**, *48*, 243–257.
- (25) Diem, M.; Romeo, M.; Boydston-White, S.; Miljkovic, M.; Matthaus, C. *Analyst* **2004**, *129*, 880–885.
- (26) Goff, K. L.; Quaroni, L.; Wilson, K. E. *Analyst* **2009**, *134*, 2216–2219.
- (27) Patel, I. I.; Shearer, D. A.; Fogarty, S. W.; Fullwood, N. J.; Quaroni, L.; Martin, F. L.; Weisz, J. *Cancer Biol. Ther.* **2014**, *15*, 225–235.
- (28) Huang, H. *Anal. Chem.* **2007**, *79*, 8281–8292.
- (29) Akram, M. *J. Cancer Educ.* **2013**, *28*, 454–457.
- (30) Jose, C.; Bellance, N.; Rossignol, R. *Biochim. Biophys. Acta—Bioenergetics* **2011**, *1807*, 552–561.
- (31) Portais, J. C.; Schuster, R.; Merle, M.; Canioni, P. *Eur. J. Biochem.* **1993**, *217*, 457–468.
- (32) Gallagher, F. A.; Kettunen, M. I.; Day, S. E.; Hu, D.-E.; Ardenkjær-Larsen, J. H.; Zandt, R. i. t.; Jensen, P. R.; Karlsson, M.; Golman, K.; Lerche, M. H.; Brindle, K. M. *Nature* **2008**, *453*, 940–943.
- (33) Gallagher, F. A.; Kettunen, M. I.; Brindle, K. M. *NMR Biomed.* **2011**, *24*, 1006–1015.
- (34) Bhargava, R.; Levin, I. W. *Appl. Spectrosc.* **2003**, *57*, 357–366.